Rotordynamic Analysis of a Large Industrial Turbocompressor Including Finite Element Substructure Modeling

J. Jeffrey Moore
Mechanical and Materials Engineering Division,
Southwest Research Institute,
Post Office Drawer 28510,
San Antonio, TX 78228-0510
e-mail: jeff.moore@swri.org

Giuseppe Vannini
e-mail: giuseppe.vannini@np.ge.com

Massimo Camatti
e-mail: massimo.camatti@np.ge.com

Paolo Bianchi
e-mail: paolo.bianchi.ing@np.ge.com

GE Oil & Gas, Nuovo Pignone,
Via Felice Matteucci, 2,
50127 Florence, Italy

A rotordynamic analysis of a large turbocompressor that models both the casing and supports along with the rotor-bearing system was performed. A 3D finite element model of the casing captures the intricate details of the casing and support structure. Two approaches are presented, including development of transfer functions of the casing and foundation, as well as a fully coupled rotor-casing-foundation model. The effect of bearing support compliance is captured, as well as the influence of casing modes on the rotor response. The first approach generates frequency response functions (FRFs) from the finite element case model at the bearing support locations. A high-order polynomial in numerator-denominator transfer function format is generated from a curve fit of the FRF. These transfer functions are then incorporated into the rotordynamics model. The second approach is a fully coupled rotor and casing model that is solved together. An unbalance response calculation is performed in both cases to predict the resulting rotor critical speeds and response of the casing modes. The effect of the compressor case and supports caused the second critical speed to drop to a value close to the operating speed and not compliant with the requirements of the American Petroleum Institute (API) specification 617 7th edition. A combination of rotor, journal bearing, casing, and support modifications resulted in a satisfactory and API compliant solution. The results of the fully coupled model validated the transfer function approach. [DOI: 10.1115/1.2938272]

Introduction

Foundation and casing effects in large frame turbomachinery typically have a pronounced effect on the resulting rotor response and the location of critical speeds. Other applications where casing effects can be important include liquid rocket engines and vertical pumps used in offshore drilling operations. Darlow et al. [1] included casing effects on a long vertical pump. Corbo et al. [2] have also presented work modeling a vertical pump with casing effects. Childs [3] presented an analysis of a rocket engine turbopump, including the flexible casing modes. Kubany et al. [4] modeled the housing and base plate of a 10 MW electric motor with 3D finite elements (FEs) and demonstrated the importance of this coupled approach to capture all of the foundation modes that lie in the operating speed range.

Most modern FE codes permit modeling rotors using 3D beam elements including gyroscopic effects. The bearings may be modeled with equivalent stiffness and damping coefficients similar to a rotordynamics code. These bearings may then be attached to a 3D FE model using solid elements representing the complex geometry of the casing and foundation. While this approach captures the true dynamic interaction between the rotor and casing, the FE model does not permit the use of speed dependent bearing coefficients, which requires much manual manipulation to generate an unbalance response plot. An alternative is to generate a transfer function, which captures the dynamics of the casing and foundation supports, and incorporate it into a rotordynamics code. The transfer function is derived from independent frequency response functions (FRFs) calculated by performing a harmonic (forced) response at each bearing housing support in each orthogonal direction (vertical and horizontal). These resulting four FRFs are then curve fitted using a modal identification algorithm that provides the transfer function in numerator-denominator polynomial format. The order of the polynomial is chosen to roughly match the number of structural modes in the frequency range of interest. This polynomial transfer function is incorporated into the rotordynamics code as a support between the bearing and ground. This approach provides the advantages of a rotordynamics code to allow a comprehensive analysis to be performed in a shorter period of time.

The subject of this study is a large size hybrid compressor (both axial and centrifugal) whose design shows so many unique features (mainly originating from the need to merge the axial part with the centrifugal part) that required a more sophisticated rotordynamics analysis to be evaluated. Basically, the compressor has a back-to-back configuration (inlet lines located at the sides of the casing and discharge lines in the middle) with the axial part located at the first inlet (see Fig. 1). The rotor is supported by tilting-pad type bearings. The power consumption is estimated at around 56 MW, provided by a steam turbine directly coupled to the centrifugal compressor shaft end with a rotational speed of 5400 rpm.

The interface between the axial and centrifugal bodies is evident in the mechanical configuration of both the casing and rotor, which will be the subject of the rotordynamic analysis that follows.

The overall casing structure is horizontally split, with the axial and the centrifugal envelopes flanged together. The axial compressor side of the casing consists of the first section that acts as both an inlet duct and bearing support, and the second section that acts as a blade carrier and mates to the centrifugal compressor casing.

The centrifugal compressor section is a large cylindrical structure, where all the radial piping connections are located (first discharge, second inlet, and discharge). The second journal bearing housing is integrated into the side portion of the casing so that the

Contributed by the International Gas Turbine Institute of ASME for publication in the JOURNAL OF ENGINEERING FOR GAS TURBINES AND POWER. Manuscript received June 1, 2006; final manuscript received October 8, 2007; published online May 18, 2010. Review conducted by Jerzy T. Sawicki. Paper presented at the ASME Turbo Expo 2006: Land, Sea and Air (GT2006), Barcelona, Spain, May 8–11, 2006.

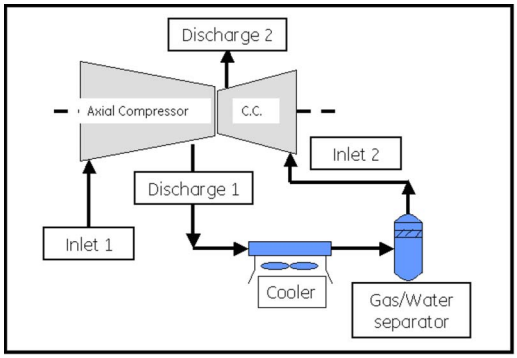

Fig. 1 Back-to-back compressor arrangement

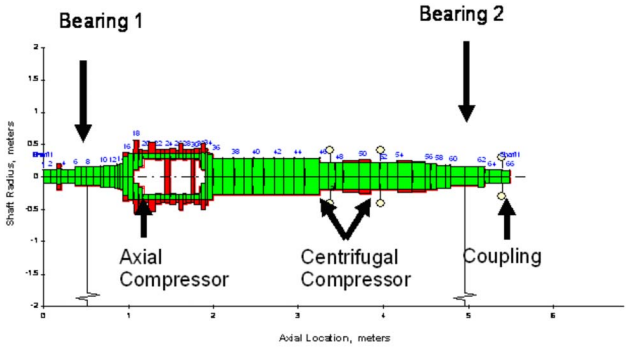

Fig. 2 Rotordynamic shaft model

bearing centerline overhang is minimized. The top and bottom halves of the casing are joined by means of a thick flange lying on the horizontal plane.

Finally, the overall casing is supported by two forward and two rear pedestals whose shape and position were the objects of the dynamic behavior optimization study.

The rotor configuration is also a result of both the integrated axial-centrifugal compressor and the specific geometric characteristics including a 10 mt total mass and around 4.5 m bearing span. The axial portion of the rotor is stacked (all the axial stage disks centered by means of a central pilot and packed together with a series of tie rods). The centrifugal portion of the casing has a traditional configuration with a solid shaft and shrink-fit components.

The primary concern in this study is to calculate the natural frequencies of the casing and determine the effect of the casing on the lateral critical speeds of the rotor. A 3D FE model for the casing is made to determine casing natural frequencies, mode shapes, and dynamic stiffness at the bearing supports. The frequency-dependent support stiffness (impedance) is incorporated into the rotordynamics model of the shaft to more accurately predict the critical speeds. Although not discussed in this paper, a full stability analysis was also performed.

Description of Modeling Approach

The analysis is divided into three parts as described below.

Part A: Rotor-Only Analysis

- build rotordynamic model of shaft, stages, bearings, seals, coupling, etc.
- perform unbalance response and stability analysis

Part B: Substructure FE Analysis

- refine solid model of casing and develop FE mesh
- perform modal analysis to obtain natural frequencies and mode shapes
- perform harmonic response analysis to obtain bearing support transfer functions
- use these transfer functions in rotor model to account for foundation effects

Part C: Combined Rotor/Casing FE Modeling

- model both rotor and casing (combined)
- used to verify results in Part B

A rotor model is prepared based on manufacturing drawings of the rotor components. Bearing models for synchronous vibration are prepared. An undamped critical speed analysis is performed followed by a damped response to unbalance based on American Petroleum Institute (API) unbalance level ($4W/N$). Overall, the following codes are used to perform the analysis:

(a) XLTRC^{2TM} Suite from Texas A&M University [5]
(b) ANSYS 9.0 (Classic and Workbench) [6]
(c) THPAD from the University of Virginia [7]
(d) TF–IDENT from the University of Virginia [8]

Rotor Model

In order to predict the rotordynamic behavior, a model is generated using a FE based rotordynamic program. Figure 2 provides a graphical definition of the mass-elastic model as used for this analysis. It consists of 66 stations and is derived from rotor drawings provided by the manufacturer.

The rotor model starts at the nondriven end at the axial compressor inlet. The coupling mass is concentrated at Station 65 of the model. The journal bearings are located at Stations 8 and 61.

The rotor model was analyzed using the XLTRC^{2TM} software developed by the Turbomachinery Laboratory at Texas A&M University. This is a FE code, which is capable of predicting undamped critical speeds and mode shapes, unbalance response, and damped natural frequencies (which provide stability information) and especially to accept support effects through transfer functions.

Tilting-pad Bearing Analysis

Bearing stiffness and damping characteristics were determined using both the THPAD software from the University of Virginia and the XLTFPBRG from the Turbomachinery Laboratory. Both codes solve the Reynolds equation. The adiabatic option in THPAD was used for these analyses and includes the effect of pivot stiffness. The energy model assumes that 100% of the hot oil exiting one pad goes into the downstream pad. The remainder of the feed oil is made up from a fresh oil supply. The same thermodynamic assumptions were valid for XLTFPBRG, but the pivot stiffness was then modeled separately. The programs were used to provide a set of synchronous coefficients for use in unbalance response analysis. THPAD was used in the first part of the analysis, while XLTFPBRG was used for the bearing study. The influence of the labyrinth seals on the critical speeds for this low pressure compressor is inconsequential; therefore, the seal effects are ignored.

Analysis of Response to Unbalance—Rigid Supports

To predict the rotor vibration amplitude and critical speed location, a response to unbalance calculation is performed using the rotor model and bearing predictions with an unbalance magnitude as defined by API 617. The unbalance is defined as $4W/N$ with units of oz in. when using lbf for weight (W) and rpm for speed (N). The equivalent equation in SI units is $6350W/N$, with units of g mm with weight in kg and speed in rpm. The results with rigid foundation supports will be presented first.

Figure 3 presents the absolute response for Bearing 1 (bell-mouth end) to one-times ($1\times$) API unbalance located at quarter-span locations (1/4 of the way in from each end) with each unbalance 180 deg out of phase from the other. The Bearing 2

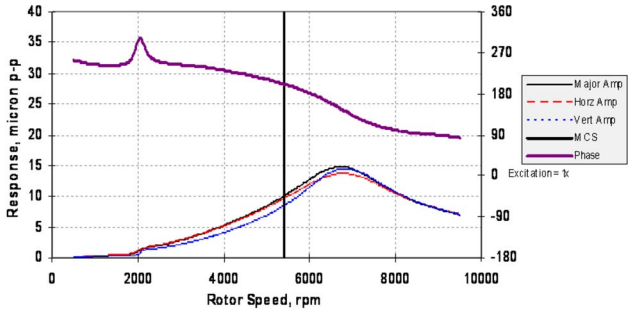

Fig. 3 Bearing 1 response unbalance at each quarter-span location (1× API)

response is not shown, but shows similar behavior with slightly less amplitude. This unbalance configuration is used to excite the second mode. Other unbalance configurations were considered, such as midspan and coupling unbalance, but will not be presented for the sake of brevity.

The peak amplitude occurs at a peak frequency of 6780 rpm and 6830 rpm for the horizontal and vertical directions, respectively. The amplification factor based on the API 617 method of half power points is between 2.40 and 2.96. The predicted separation margin to the maximum continuous speed (MCS) is 26%, satisfying API requirements of 15%. The phase angle curve is also shown in Fig. 3 for reference. Note that these results are for a rigid foundation support.

All the response predictions are at nominal bearing conditions. While the results above demonstrate adequate separation margin to the second critical speed, these results assume a rigid bearing support. Due to the unique design of the unit with a hybrid axial compressor mated to a two-stage centrifugal compressor, a more rigorous analysis is performed. The flexibility of the bearing supports is modeled using a 3D FE model of the complex casing and includes the pedestal support effects. Many different designs were considered and will be discussed in greater detail later.

Casing and Foundation Support Analysis

Starting with solid models, a FE mesh is developed using ANSYS WORKBENCH™. Figure 4 shows the solid model assembly with the top casing half removed for the original design configuration. The difference in scale and weight of the two casings makes this design unique with dynamics that are not intuitive. The structural parts of the casing and supports are the exact geometry. Only small features, such as bolt holes and some fillets, have been removed to reduce the complexity of the model. The internal diaphragm components in the centrifugal section have been simplified by generating new solids with similar mass distributions.

Once the assembly is created, it is imported into the FE software and a mesh is generated. The resulting grid that was generated for the original casing geometry is shown in Fig. 5. The geometry includes both the forward and aft pedestal mounts to improve the accuracy of the predictions. Bonded contact elements are used between the various components, which represents continuous contact between the objects. The model contains 261,000 grid points. This model incorporates some stiffening members of the axial and centrifugal casings to improve the stiffness of this interface joint, as shown in Fig. 4.

Figure 6 shows the boundary conditions that were utilized in the model. All 4 ft of the pedestals were constrained (rigid foundation is assumed). The "Gib-Key" located at the bottom of the axial compressor casing provides horizontal (only) constraint. The bellows type connections to the nozzles were studied and found to provide negligible effect on the natural frequencies. Therefore, they were ignored (i.e., no connection).

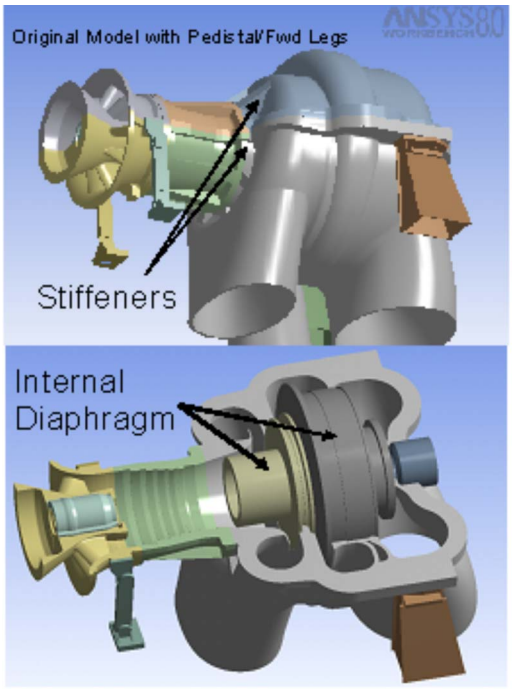

Fig. 4 Solid model assembly—original casing geometry

In order to determine the dynamic stiffness of the support structure, a harmonic (forced) response was performed for each bearing and orthogonal direction (vertical and horizontal) resulting in four independent calculations. Figure 7 shows the location of the force for the Bearing 1 vertical case. The upper half of the bell mouth has been removed for visual purposes in the figure. The displacement at the bearing support where the force is applied is calculated using a harmonic solution (forced response) of the finite element analysis (FEA) model. By dividing the force by this displacement, the dynamic stiffness transfer function is calculated. This transfer function is frequency dependent due to the presence of the casing modes in the frequency range of interest. A curve fit of the FRFs is performed to generate a high-order polynomial in transfer function form containing both a numerator and a denominator. As said before, the rotordynamics code accepts these transfer functions to include the casing effects in the unbalance response and critical speed predictions. This approach will be further explained in subsequent sections.

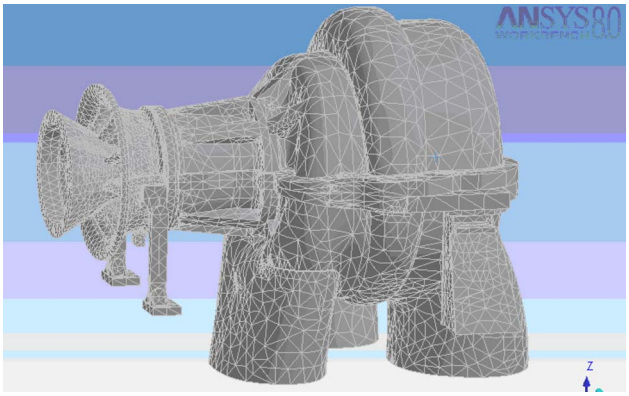

Fig. 5 FE mesh—original casing geometry

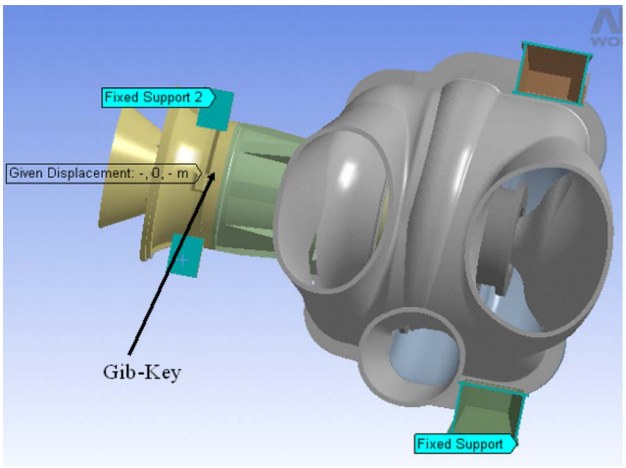

Fig. 6 Boundary conditions

Modal Analysis Results

A modal analysis solves the following eigenvalue problem for the casing and pedestal support model above:

$$[[K] - \omega^2[\mathbf{M}]]\{X\} = \{0\} \tag{1}$$

where, K and $\mathbf{M}$ are the stiffness and mass matrix, respectively, and ω is the undamped natural frequency.

The solution to the eigenvalue problem results in the undamped natural frequencies and mode shapes of the casing structure (absent the rotor model). The analysis reveals if any casing natural frequencies will be near the operating speed of 5400 rpm. Furthermore, a natural mode with motion near the bearing supports may adversely soften the support, thereby affecting the rotor critical speeds. As presented above, the second critical speed is above the running speed using a rigid support assumption. Any softening of the bearing support may drop the critical speed close to the running speed. Furthermore, the modal solution is a necessary step for performing the harmonic analysis described later.

Figure 8 shows the mode shapes for the first several casing modes. Not shown are the first two rigid body modes in the axial and horizontal directions, where only the pedestals are flexing. The results show several modes in the frequency range of interest starting with the casing first bending and bell-mouth modes in the vertical direction. These modes, however, occur at a speed well below the running speed and at a frequency low enough that the rotor will likely not excite these modes (this will be confirmed later). There are other modes near the operating speed of 5400 rpm, including the Bearing 2 drum mode (axial drum motion), first bending in the horizontal direction, and the second bell-mouth vertical mode. This last mode is close to the calculated second rotor critical speed and will likely interact with the rotor.

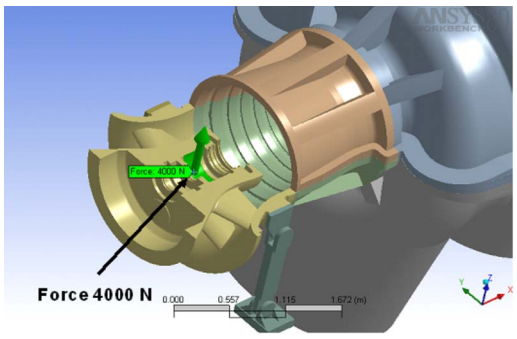

Fig. 7 Location of applied force for harmonic analysis

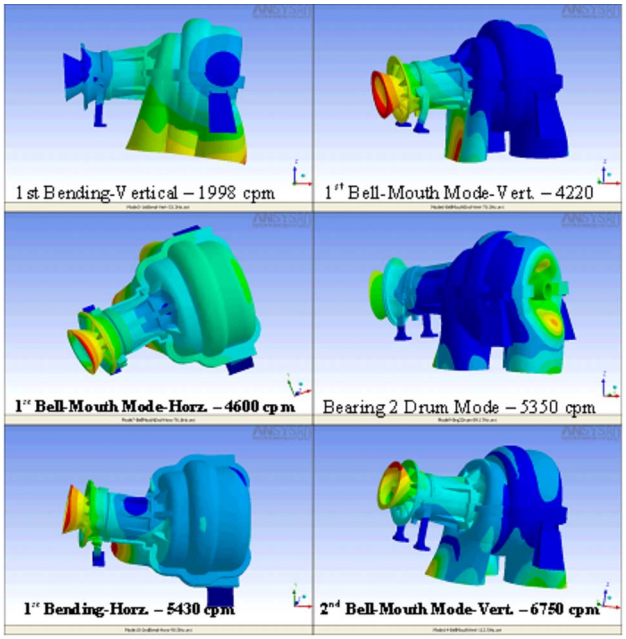

Fig. 8 Calculated mode shapes and natural frequencies—original casing model

Harmonic Analysis

In order to predict the dynamic stiffness of the casing and support structure, a harmonic (forced) response analysis is performed. As described previously, a harmonic force is applied at each bearing support in each lateral direction (horizontal and vertical) requiring a total of four calculations. Due to the large size of the model, mode superposition is employed. This technique normalizes the first N number of modes to decouple the system of equations resulting in modal mass and modal stiffness vectors defined as

$$\mathbf{M}_r = \phi_r^T[M]\phi_r$$

$$\mathbf{K}_r = \phi_r^T[K]\phi_r \tag{2}$$

where, φ_r is the eigenvector (mode shape) for mode (r), $\mathbf{M}_r$ and $\mathbf{K}_r$ are the modal mass and stiffness for mode (r), respectively.

For this problem, the first 40 modes are used, which cover up to twice the maximum frequency range of interest. The decoupled system may now be solved using single-degree-of-freedom (DOF) techniques in modal space, and then transformed back into physical space. Mode superposition is an option available in ANSYS. The response is calculated from zero to twice the running speed (10,800 cpm) in 120 rpm steps. This method requires a damping ratio to be assumed. A value of 2% was used for all calculations and is typical of steel structures based on the authors' experience.

Figure 9 shows the response output for an excitation of 4000 N, which was arbitrarily chosen but is representative of the dynamic force transmitted from the bearings due to the imbalance of the rotor. Since this force will be normalized by the resulting displacement and the model represents a linear system, the magnitude of the force is not important. The first bell-mouth vertical mode near 4200 rpm is the most pronounced followed by the Bearing 2 drum mode at the running speed (5400 rpm). This mode has a vertical component near Bearing 1, which causes this mode to be excited. The second bell-mouth-vertical mode near 6700 rpm can be observed in Fig. 9 as well, but is much less excited. Nevertheless, it does act to reduce the dynamic stiffness at a frequency near the second rotor critical speed where it is needed.

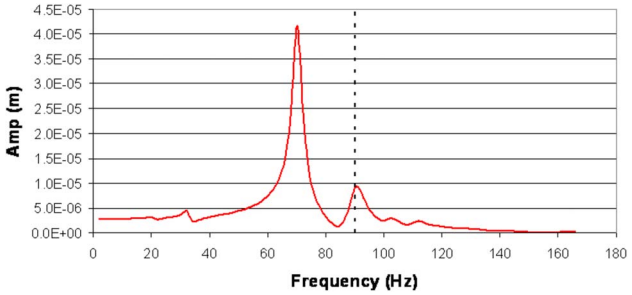

Fig. 9 Forced response prediction—Bearing 1-vertical—original casing model

Using this response result, the dynamic stiffness transfer function is calculated by dividing the excitation force (4000 N) by the displacement shown in Fig. 9. This result is shown in Fig. 10. A sensitivity study from the rotor model determined that the minimum required stiffness to provide second critical speed separation margin is about 5.0E+09 N/m. Therefore, the stiffness in the range near 6700 rpm should exceed this value. The original casing model fell short of this value in this frequency range.

In order to incorporate the predicted dynamic stiffness into the rotordynamic model, a curve fit is performed to create a polynomial in generic transfer function format

$$K_d(\omega) = \frac{a_0 + a_1\omega + \ldots + a_m\omega^m}{b_0 + b_1\omega + \ldots + b_n\omega^n} \tag{3}$$

Curve Fitting of Frequency Response Functions

A software program known as TF–IDENT [8] was used to perform the curve fit. Care was taken to ensure that a good fit was made and that the roots of the polynomial were stable (negative real part). Figure 11 shows the resulting transfer functions and the closeness of the fit (solid line is curve fit). Only direct transfer functions are calculated (i.e., no cross DOF FRFs are used from one bearing support to another). This assumption was justified by noting minimal influence of the cross DOF terms when included.

Rotordynamic Analysis With Foundation Effects

The transfer functions derived in the previous section were incorporated into the XLTRC^2 rotordynamics model: This code permits incorporation of transfer functions between two stations (typical for modeling of magnetic bearings and foundation supports). The fundamental assumption of this approach is that the casing and rotor modes are decoupled. In other words, the frequency and mode shape of the casing is not affected by the rotor, since the rotor was not included in the FE model of the casing. This assumption will be validated by comparing the results to the fully coupled model presented later in this paper. This assumption

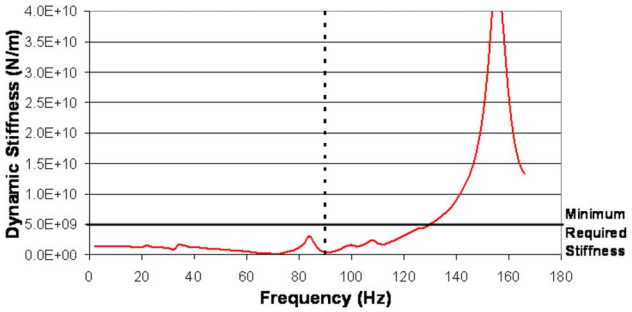

Fig. 10 Dynamic stiffness prediction—Bearing 1-vertical—original casing model

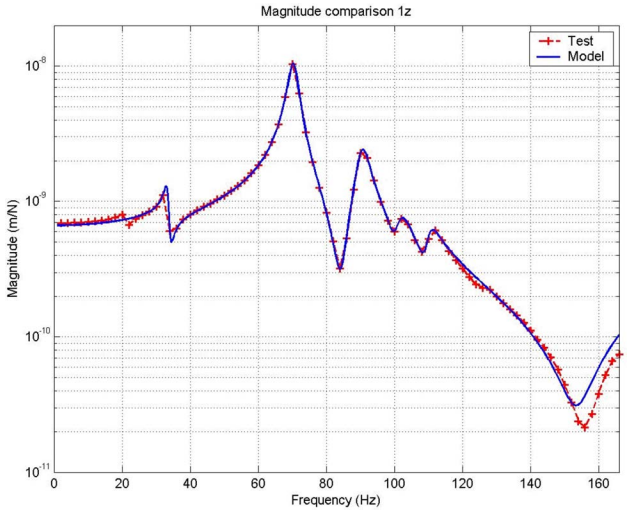

Fig. 11 Curve-fit of FRFs—original casing model

is not to be confused with component mode synthesis in which independent reduced order models of the rotor and casing are coupled through master degrees of freedom.

Figure 12 presents the absolute (not relative) response to the same API quarter-span unbalance as used in the rigid foundation case. The peak amplitude occurs at peak frequencies of 5090 rpm and 5260 rpm for the horizontal and vertical directions, respectively. The amplification factor based on the API 617 method of half power points is between 10.9 and 16.2. The predicted separation margin to the MCS is 2.6%, which does not satisfy the API requirement of 25.8%, calculated using the amplification factor. The casing first Bending-vertical mode near 4200 rpm is excited, as shown in Fig. 12. Note that these results include the original casing foundation support model. The casing flexibility, especially at the forward bearing, has caused the second rotor critical speed to drop near the operating speed. Clearly, further modifications of the casing are required.

Description of Design Modifications

To improve the rotor support stiffness and move the casing modes away from the operating speed, both the casing and support stiffness are modified. Fig. 13 shows the first alternate design, which incorporates a cradle type forward support along with additional ribs on the inlet and centrifugal casing. It was identified from the previous mode shapes that a significant amount of bending was occurring at the junction between the axial and centrifugal compressor casings. The diameter of this interface was further

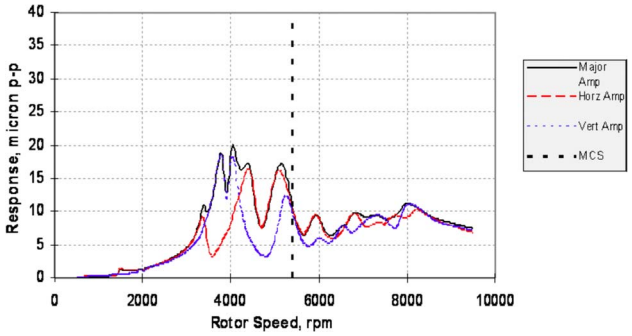

Fig. 12 Bearing 1 response unbalance at quarter-span location (1× API)—original casing model

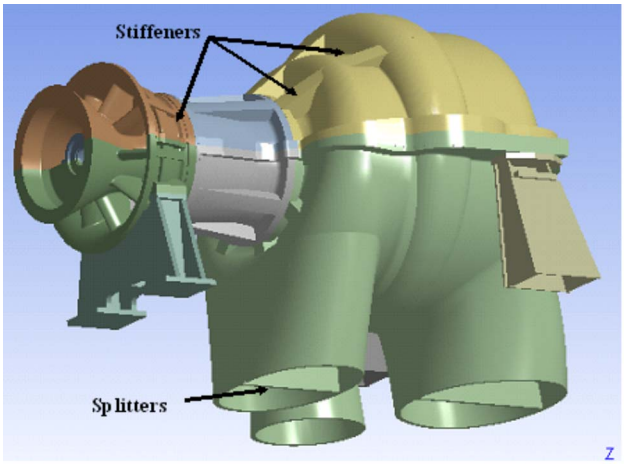

Fig. 13 Modified casing with cradle support

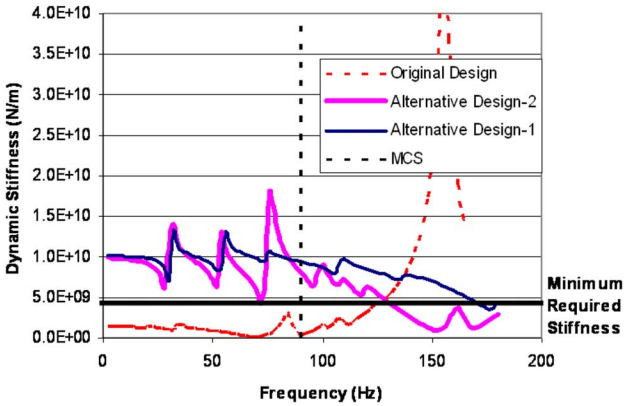

Fig. 15 Dynamic stiffness comparison

increased as well. In an effort to improve the load path through the axial compressor discharge nozzle and the centrifugal inlet nozzle, splitter plates were added, as shown in Fig. 13.

A second alternate design is presented in Fig. 14, which utilizes additional stiffeners in the inlet, axial, and centrifugal casings. This design also employs a pedestal type support at the forward mounts. This design utilizes the thicker pedestal supports. The nozzles are changed by adding flanges along with the splitters, as well as a stiffener connecting two of the nozzles. These features help to move the bell modes of the nozzles out of the operating speed range.

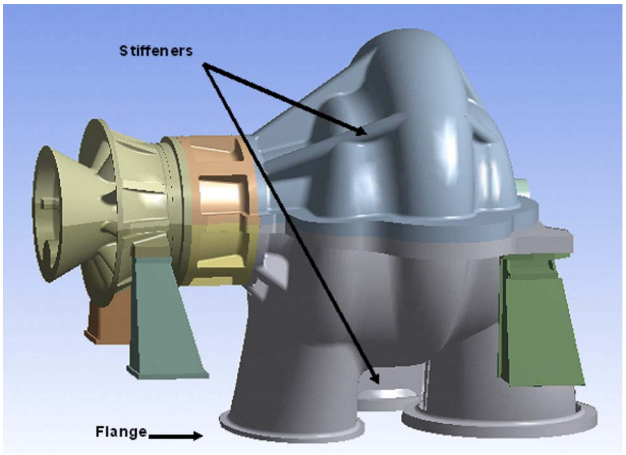

Fig. 14 Modified casing with forward pedestal supports

Modal Analysis of Modified Designs

Table 1 summarizes the modal analysis of these modified designs. The cradle mount design increases the first bending frequency, especially in the vertical direction compared to the original design but is still below the running speed. The bell-mouth mode in the vertical direction has significantly increased to well above the running speed (10,700 cpm). This design provides significantly more vertical stiffness than the original design with pedestal leg supports. The horizontal frequency is increased as well, but results in a location slightly above the running speed. This will have an adverse effect on the second horizontal critical speed of the rotor, which will be presented next.

Alternate Design 2 results in a good increase in the bell-mouth vertical modes, but places the horizontal first bending mode just above the running speed.

Critical Speed Analysis of Modified Designs

Transfer functions were derived for these designs and implemented in the XLTRC^2 model, as described above. Figure 15 compares the dynamic stiffness of the forward bearing support for the three configurations. Both alternate Designs 1 and 2 meet the

Table 1 Summary of modal analysis of modified designs (casing only absent rotor) (frequency in cpm)

Mode	Description of Mode	Original Design	Alternate Design-1	Alternate Design-2
1	Rigid Mode-Axial	1298	1833	1764
2	Rigid Mode-Horizontal	1566	1584	1386
3	1st Case Bending Vertical	1998	3249	3139
4	1st Case Bending Horizont	3444	3604	6480
5	Bell Mouth Mode-Vert	4217	10705	9136
6	Bell Mouth Mode-Horz	4599	6937	
7	2nd Case Bending-Horz	5431		
8	Bell Mouth Vert / Internal M	6750		
9	Bell Mouth Mode-Vert-2			10099

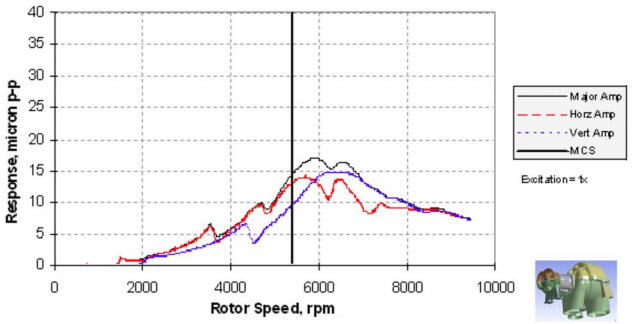

Fig. 16 Bearing 1 response to API unbalance at quarter-span location for alternate Design 1

minimum required stiffness in the vertical direction. Unfortunately, neither design meets this value in the horizontal direction.

Figure 16 shows the resulting unbalance response using quarterspan, out-of-phase unbalance to excite the second rotor critical speed for alternate Design-1. The results show an improvement over the original casing design, but the horizontal critical speed is close to the running speed.

Alternate Design-2 includes additional stiffening of the casings and pedestal supports. Figure 17 provides the unbalance response calculations of Bearing-1 for this design. The second critical speed in the vertical direction has improved to acceptable levels. However, the horizontal critical speed remains close to the running speed. The casing modes are sufficiently away from the running speed.

Table 2 summarizes the calculated critical speed and amplification factor and compares the separation margin to API requirements for these different cases. The table shows that alternate Design-2 has a critical speed in the vertical direction almost as high as alternate Design-1 but with a better horizontal critical speed margin. The separation margin is met in the vertical direction for alternate Design-2 but still falls short of some of the API requirements in the horizontal direction.

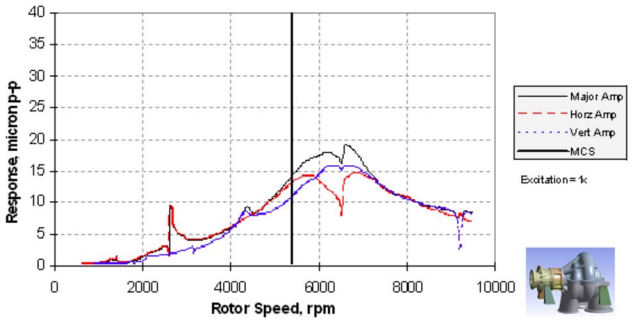

Fig. 17 Bearing 1 response to API unbalance at quarter-span location for alternate Design 2

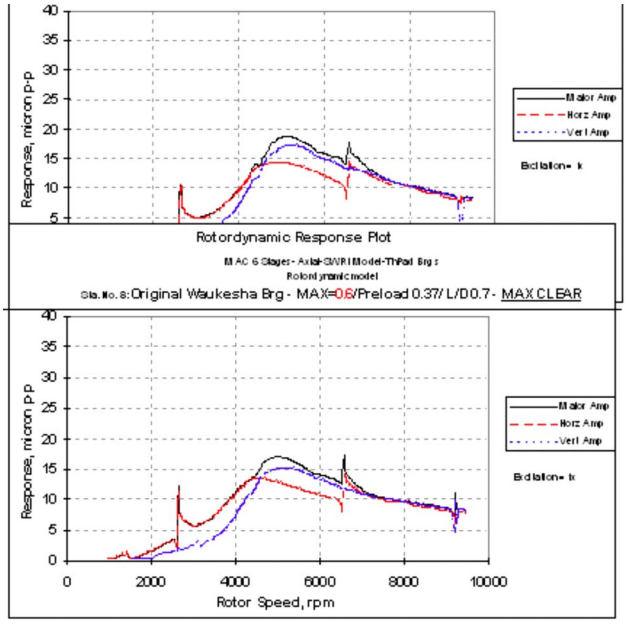

Fig. 18 Bearing 1 response to API unbalance at quarter-span location for alternate Design 2 with modified bearings, minimum and maximum clearance

Modified Bearing Study

Since further improvements in the foundation stiffness are not possible without major modifications to the casing structure, the amount of improvement with alternate bearings was investigated. The result of this study is included here. The casing model used is alternate Design 2. The bearing modification consists of increasing the assembled clearance while maintaining the preload constant. All other bearing parameters are held constant. The larger clearance results in softer bearings that reduce the second critical speed to a value less than the running speed. The amplification factor is reduced, as shown in Fig. 18, which provides the response of Bearing 1 for both minimum and maximum bearing clearances. Since the amplification factor is less than 2.5, no separation margin is required. Comparing Fig. 18 to the Bearing 1 response of Fig. 17, the response to unbalance is slightly higher for the modified bearing case but meets API requirements.

Table 3 compares the Bearing 1 critical speeds of the modified bearing at minimum and maximum clearances with the nominal (average) clearance case for the original bearing. The results show that the modified bearing meets API requirements for separation margin. The coupled solution that will be presented in the next section shows that the actual critical speed of the coupled rotor/casing system should be even lower than the transfer function method indicates. Therefore, the separation margin will be even more favorable than the values shown in Fig. 18.

Table 2 Summary of critical speeds with alternate designs

	Rigid foundation		Original design		Alternalte Design 1		Alternate Design 2	
	Vert	Horz	Vert	Horz	Vert	Horz	Vert	Horz
Second	6830	6780	5290	5150	6580	5680	6500	5840
Amp. factor	3.0	2.4	16.4	11.0	2.8	3.0	2.8	3.9
Sep. margin	27%	26%	–2%	–5%	22%	5%	20%	8%
API req. S.M.	15%	0%	16%	15%	14%	15%	14%	20%

Table 3 Summary of critical speeds with modified single casing and modified bearings

			Original Bearings-nom Clearance		Modified Bearings-min Clearance		Modified Bearing-max Clearance	
	Vert	Horz	Vert	Horz	Vert	Horz	Vert	Horz
Second critical spd	7180	7140	6500	5840	5240	4940	5180	4520
Amp. factor	3.01	2.40	2.80	3.91	1.92	2.06	1.88	1.70
Sep. margin	33%	32%	20%	8%	−3%	−9%	−3%	−9%
API req S.M.	16%	0%	14%	20%	Not req	Not req	Not req	Not req

Table 4 Summary of rotor and casing undamped natural frequencies—alternate Design-1

Mode	Rotor only (cpm)	Casing only (cpm)	Casing/rotor combined model (cpm)
First rotor critical Horz/Vert	2100/2140		1980/1960
First casing mode Horz/Vert		3600/3250	3540/3250
Second rotor critical Horz/Vert	5580/5870		4990/5470
Bell mouth mode Horz/Vert		6940/10700	7110/10700

Coupled Rotor and Casing Finite Element Model Results

This section describes the results of "Part C," as shown above. The FE beam model of the rotor is coupled to the casing and a combined solution is calculated using ANSYS. This most general approach captures the interactions between the rotor and the casing and is more general than the "one-way" coupling described above. Although the model is more difficult to build, this coupled approach is used to validate the results presented in the previous section. Before analyzing the coupled rotor-casing problem, the rotor-only model was run in ANSYS as a beam element model and resulted in identical results to XLTRC^2, thereby validating the ANSYS rotor model.

Coupled Rotor-Casing Model—Alternate Design-1

The rotor is coupled to alternate Design 1, as described above. Figure 19 shows the resulting FE model. Beam elements are used to simulate the rotor.

Modal Analysis of Coupled Model—Cradle Casing Design

Table 4 compares the rotor and casing undamped natural frequencies of the coupled rotor-casing model with the rotor-only and casing-only models. Adding the additional compliance and inertia of the casing reduces both the first and second rotor critical speeds. First, bending modes of the casing also decrease slightly (horizontal direction) when the rotor is added. However, the bell-mouth mode increases in the horizontal direction and stays unchanged in the vertical direction. This increase is attributed to the fact that the rotor and casing are moving out of phase for the bell-mouth mode.

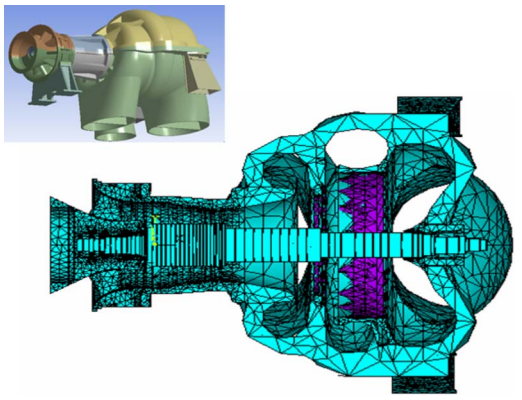

Fig. 19 Coupled rotor-casing model—alternate Design 1

Harmonic Response of Coupled Model—Cradle Casing Design

A forced response for the quarter-span (out-of-phase) case is applied to the coupled model equal to a 1× API unbalance as before. The ANSYS results are scaled to provide an $m \cdot e \cdot \omega^2$ unbalance excitation, where m is the unbalance mass, e is the unbalance eccentricity, and ω is the running speed. Since ANSYS does not permit speed dependent stiffness and damping coefficients, a constant bearing stiffness is used that is iterated to match the second critical speed in the resulting calculations. The effect of gyroscopics on this beam-style rotor is minimal and is ignored. Figure 20 compares the vertical rotor response at the bearings between the ANSYS combined rotor/casing FEA model, the XLTRC^2 rotor model using transfer functions derived from the FEA casing-only model, and the XLTRC^2 rotor model with rigid foundation supports (rotor only).

The vertical response in Fig. 20 shows that the critical speed reduces with the additional casing compliance of the XLTRC^2 model with transfer functions compared to the model with a rigid foundation. The coupled rotor-casing model shows an even larger drop in the predicted frequency. The response to unbalance amplitudes is similar for the various models, with the XLTRC^2 model with transfer functions showing generally higher amplitude.

Overall, the response behavior is similar for the combined rotor/casing model compared to the transfer function approach. This result validates the previous use of transfer functions to capture the rotor-casing dynamics.

Table 5 summarizes the critical speeds from the unbalance response calculations for alternate Design 1. In addition, the amplification factor, separation margin, and required API separation margin are shown. The results show that the compressor easily meets API requirements when a rigid foundation is used. Using

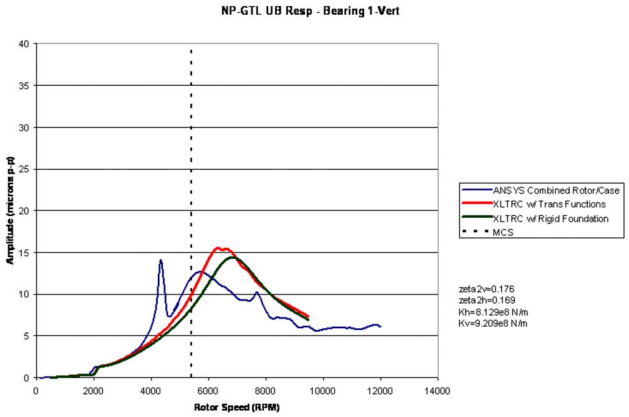

Fig. 20 Unbalance response comparison—Bearing 1 vertical response

Table 5 Critical speed summary of three modeling approaches

	XLTRC-rigid foundation		XLTRC-with transfer funct.		ANSY-comb rotor/casing	
	Vert	Horz	Vert	Horz	Vert	Horz
Second critical spd	6830	6780	6580	5680	5700	5220
Amp. factor	2.96	2.40	2.84	2.96	1.94	2.48
Sep. margin	27%	26%	22%	5%	6%	−3%
API Req S.M.	15%	0%	14%	15%	0%	1%

the XLTRC^2 model with transfer functions, the separation margin is met in the vertical direction, but not the horizontal as previously presented. The amplification margin with the ANSYS coupled model is slightly less than 2.5, which does not require a separation margin. Although the transfer function model overpredicts the critical speeds, this technique permits easier modification of the rotor system and faster analysis time since a conventional rotor code is being employed.

Conclusions

The purpose of this study was to determine the effect of casing and foundation dynamics on the rotordynamic shaft response for a large hybrid axial/centrifugal air compressor. The system contains casing modes both below and above the design operating speed. Some of these modes can be excited by the rotor system. However, more importantly, the compliance of the casing due to the presence of these modes caused the second rotor critical speed to drop unacceptably close to the operating speed. Several modifications to the casing were investigated, greatly improving the rotor response and the separation of the casing modes from the running speed. However, the separation margin of the second critical speed still did not meet API requirements. A further modification of the tilting-pad journal bearings demonstrated an acceptable design.

To verify the method that uses transfer functions to represent the casing dynamics, a fully coupled rotor/casing/foundation FE model is created in ANSYS. This model more accurately captures the interaction between the rotor and casing modes but is more computationally intense. The results show similar levels of unbalance response but critical speeds slightly lower than when transfer functions are used. Final confirmation of the transfer function model with a fully coupled model is recommended.

The design finally chosen (alternate Design 2 with modified bearings) involved stiffening the casing, foundation, and modifying the tilting-pad journal bearings. It is acceptable both from the point of view of the API (respect of proper separation margins) and the manufacturer (acceptable unbalance sensitivity and limited amplification factor even without bearing tuning).

Due to the unique features of this compressor, the advanced analytical approach presented here was applied with the aim of enhancing traditional rotordynamic methods. This advanced methodology permitted the discovery of a potential concern with the second critical speed early in the development cycle, allowing relatively inexpensive design modifications to be implemented. The ability of the tools to interface directly with the 3D solid models of the compressor further reduced the analysis cycle time.

Acknowledgment

The authors would like to thank Guoxin Xi and Hunter Cloud of BRG Consulting for their assistance in performing the transfer function curve-fits. Thanks also goes to Dr. Anthony Smalley for his advice on the project, and to Eugenio Rossi and Stefano De Gaetano of Nuovo Pignone who worked proactively with the authors helping to reach such a positive conclusion. Finally, our appreciation goes to the management of both Southwest Research Institute® and GE's Oil & Gas business for their permission to publish this work.

References

[1] Darlow, M. S., Smalley, A. J., and Ogg, J., 1978, "Critical Speeds and Response of a Large Vertical Pump," ASME Paper No. 78-PVP-34.
[2] Corbo, M. A., Stefanko, D. B., and Leishear, R. A., 2002, "Practical Use of Rotordynamic Analysis to Correct a Vertical Long Shaft Pump's Whirl Problem," *Proceedings of the 19th International Pump Users Symposium, Turbomachinery Laboratory*, Texas A&M University, College Station, TX, pp 107–120.
[3] Childs, D., 1978, "The Space Shuttle Main Engine High Pressure Fuel Turbopump Rotordynamic Instability Problem," ASME J. Eng. Power, **100**, pp. 48–57.
[4] Kubany, J. S., Tecza, J. A., and Gustafsson, P., 2003, "Dynamic Evaluation of a Three Point Mount Baseplate for a Motor Driven, Centrifugal Compressor Package," ASME Paper No. DETC2003/VIB-48463.
[5] 2001, XLTRC^{2TM} SUITE, Version 2.1, Turbomachinery Laboratory, Texas A&M University.
[6] 2004, ANSYS, Version 9.0 (Classic and Workbench), ANSYS, Inc.
[7] 1999, THPAD, Version 2.63, A manual for use with the tilting pad bearing Program THPAD, Rotating Machinery and Controls Industrial Research Program, University of Virginia, ROMAC Report No. 284.
[8] TF-IDENT User Manual, Rotating Machinery and Controls Industrial Research Program, University of Virginia.